Methods to Perform High Velocity LTE Experiments at Low Velocities

Martin Lerch
Institute of Telecommunications,
TU Wien, Vienna, Austria
Email: mlerch@nt.tuwien.ac.at

José Rodríguez-Piñeiro, José A. García-Naya,
and Luis Castedo
University of A Coruña, A Coruña, Spain
Email: {j.rpineiro, jagarcia, luis}@udc.es

***Abstract*—LTE is designed to support user velocities of up to 500 km/h where experiments are expensive, time-consuming and dangerous. Fortunately, such experiments can be emulated at lower velocities by time-stretching the transmit signals. This method preserves the spatial properties of the mobile radio channel but performs a spectral compression. In this paper, we propose a new set of methods that preserve the spectral properties by inserting additional subcarriers. Next, we compare the method of time-stretching to the new set of methods by applying them to LTE downlink signals. We evaluate the properties and the main drawbacks of the proposed methods by simulations using standard-compliant LTE signals. Finally, we highlight practical aspects to be considered when implementing the proposed high speed emulation techniques.**

I. Introduction

Mobile communications experiments in high mobility environments such as high speed trains, motorways or airplanes are expensive, time-consuming and sometimes dangerous or even impossible. Researchers are then often forced to rely on simulations and their underlying models to test new transmission or receiver techniques. Our novel approach is to perform experiments in the real environment at lower velocities. Higher velocities are then emulated by time stretching of the transmit signals before the transmission and corresponding time compression in the receiver. When stretching a data symbol with duration T_s by a factor I and moving at the reduced velocity $\frac{v}{I}$, the spatial length of the symbol $\Delta z = vT_s = T_s \cdot I \cdot \frac{v}{I}$ is the same as if the original symbol was transmitted at v. Considering Orthogonal Frequency Division Multiplexing (OFDM) as modulation scheme, time stretching by a factor I corresponds to a reduction of the subcarrier spacing $\Delta f = \frac{1}{T_s}$ by the same factor I. Therefore, the effect of Inter-Carrier-Interference (ICI) due to Doppler shifts is emulated correctly as the Signal-to-Interference Ratio (SIR) [1] due to ICI is a function of the maximum relative Doppler shift $f_{\mathrm{D,max}} = \frac{f_c \cdot v}{c \cdot \Delta f} = \frac{f_c}{c} \cdot \frac{I}{\Delta f} \cdot \frac{v}{I}$ and remains unchanged for a fixed carrier frequency f_c and a fixed propagation velocity c. Besides the intended decrease of the subcarrier spacing to correctly emulate the ICI, this spectral compression also changes other spectral parameters of the transmit signal. In case of 3GPP Long Term Evolution (LTE) [2] downlink transmissions, where OFDM is used as modulation scheme, these parameters are the transmit bandwidth and the spectral spacing of the reference symbols (pilots).

This method of time stretching OFDM signals to emulate higher velocities was used in [3] to experimentally test ICI-aware OFDM receivers and in [4] where ICI-cancellation techniques were evaluated. Furthermore, this method was validated by measurements under controlled laboratory conditions [5]. Finally, in [6] the results were compared to results obtained by simulations based on channel models reflecting high speed train scenarios. Although these tests yielded promising results, we were interested in the limitations of this technique and to develop alternative methods that preserve the bandwidth and the pilot spacing of LTE downlink signals. In this paper, we propose a set of new methods that stretch OFDM signals in a different way. Instead of resampling in the time domain, the symbol length is increased by increasing the FFT length in the frequency domain by inserting additional subcarriers between the original ones. Section II gives a detailed description of the different methods considered. In Section III the applicability and the limitations of the different methods are shown by simulations before practical aspects are discussed in Section IV. In Section V, all findings are summarized.

II. Methods

We divide the methods considered for comparison into two sets of methods as illustrated in Figure 1. These are methods based on signal resampling on the one hand, and methods that insert additional subcarriers on the other hand.

A. Changing the sampling rate

The simplest method to change the length of a given OFDM signal to any value higher or lower than the initial length by a factor I is to change the sampling rate at both, the transmitter and the receiver by the same factor $\frac{1}{I}$. In its basic implementation (*method 1*) this method is completely transparent to the communication system so there is no need for any modifications in the implementation of the actual system except for a change in sample rate. In order to validate this method by measurements, we introduced a modified method (*method 2*) in [6]. Under the constraint of an integer factor $I>1$ the resampled signal is repeated I times in order to occupy the same total bandwidth as the original signal. Measurement results for all signals are then averaged preserving the Signal-to-Noise Ratio (SNR). Repeating exactly the same signal, results in an increase of the Peak-to-Average Power Ratio

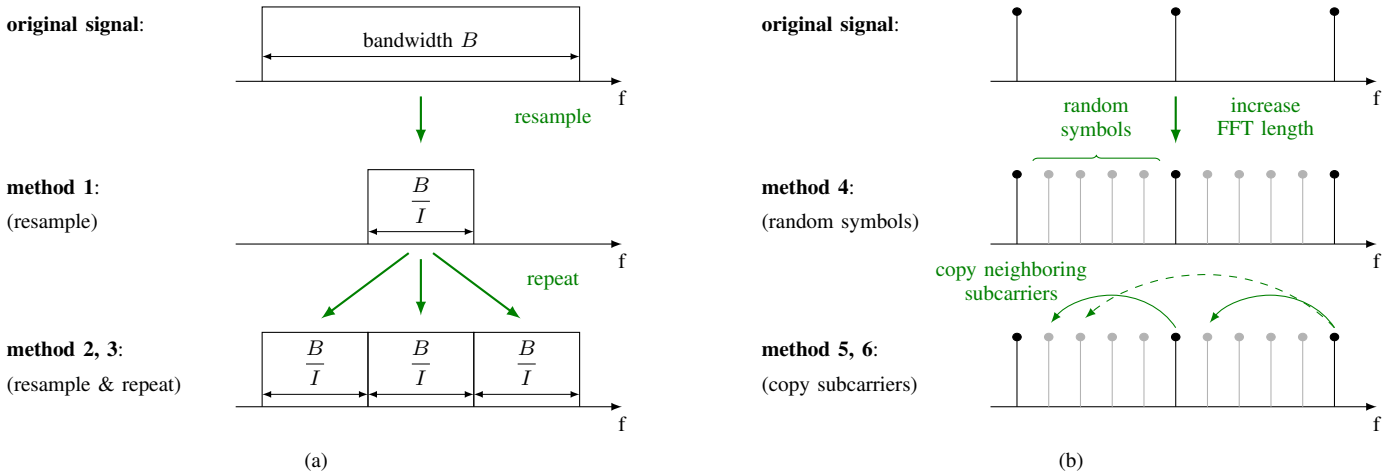

Fig. 1. Methods to decrease the subcarrier spacing of an OFDM signal: (a) Resampling. (b) Increasing the FFT length and inserting additional subcarriers.

(PAPR) as shown in Section IV. Therefore, we also consider *method 3* where different realizations of the same signal are repeated.

B. Inserting additional subcarriers

In order to preserve the bandwidth and the pilot spacing, we propose a second set of methods to time-stretch an OFDM signal. As illustrated in Figure 1b, the FFT length, that is the total number of subcarriers (including guard subcarriers at the edges) passed to the IFFT in the OFDM modulator, is increased by an integer factor $I>1$ by inserting $(I-1)$ additional subcarriers between the original ones. By keeping the initial sampling frequency, the symbol length is thereby increased by the factor I and the subcarrier spacing is decreased by the same factor. At the receiver side, the additional subcarriers are discarded after the FFT in the OFDM demodulator. The choice of the symbols being modulated onto the additional subcarriers depends on the application. If only the average ICI level shall be emulated, random symbols from the symbol alphabet used for the actual data symbols are used (*method 4*). ICI cancellation algorithms can not perform correctly in this case since the interference is not caused by the original neighboring subcarriers. We consider this problem in *method 5* where the initial neighboring subcarriers are copied to the appropriate positions in order to generate the correct ICI. The number of correct neighbors is then limited to $\lfloor \frac{I}{2} \rfloor$[1]. The drawback of this method is its increased PAPR as the subcarriers are not independent anymore (see Section IV). Therefore, we include *method 6* into our comparison where only the adjacent neighbor is copied and random symbols are used for the remaining subcarriers.

III. Simulation based comparison

In order to show the applicability and the limitations of the different methods discussed in this paper, we performed simulations using a modified version of the Vienna LTE Downlink Link Level Simulator [7], [8]. First, we transmit the original signal at receiver velocities of v=50, 100, 200 and 400 km/h. Then, the modified signals are transmitted at 50 km/h to emulate transmissions at v=100 km/h (I=2), 200 km/h (I=4) and 400 km/h (I=8). We use two different channel models, both based on a modified version [9] of the Zheng model [10] for time-variant channels. Thereby, the *Pedestrian B* (PedB) channel model [11] implements frequency selective channels while *flat Rayleigh* channels consist of a single channel tap and are therefore frequency flat. The channel estimation in the receiver used is performed using least squares channel estimation with linear interpolation.

A. Signal to interference ratio

The SIR is obtained by setting subcarriers that are not too close to each other and not too close to the spectral edges of the signal to zero. The SIR is then calculated by obtaining the signal plus interference power P_{SI} at the non-zero data subcarrier positions $\mathcal{D}$ and the interference power P_I at the zero subcarrier positions $\mathcal{Z}$ as

$$SIR(v,I) = \frac{\overline{P}_{SI} - \overline{P}_I}{\overline{P}_I} = \frac{\overline{P}_{SI}}{\overline{P}_I} - 1 \tag{1}$$

$$= \frac{\frac{1}{|\mathcal{D}|}\sum_{r=1}^{R}\sum_{n=1}^{N}\sum_{k\in\mathcal{D}} |\hat{a}_{n,k,r}(v,I)|^2}{\frac{1}{|\mathcal{Z}|}\sum_{r=1}^{R}\sum_{n=1}^{N}\sum_{k\in\mathcal{Z}} |\hat{a}_{n,k,r}(v,I)|^2} - 1, \tag{2}$$

whereas $\hat{a}_{n,k,r}$ is the received symbol after the FFT in the demodulator at subcarrier k, time symbol n and channel realization r. In Figure 2, the simulation results are compared to the analytical result [1] for the Jakes' spectrum the used channel models implement. The results for all methods that resample the original signal coincide with the desired result for the original signal and the analytical result. For the second set of methods, where additional subcarriers are inserted, only the method that inserts random symbols properly emulates the average SIR. We observe higher interference power for the

[1]For even I we randomly choose one of the two possible subcarriers for the center position.

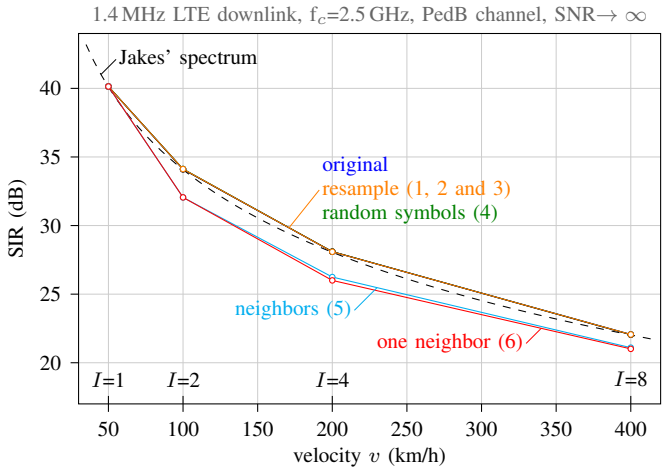

Fig. 2. All methods that keep data symbols independent emulate the SIR correctly. Repeating data symbols increases the interference power.

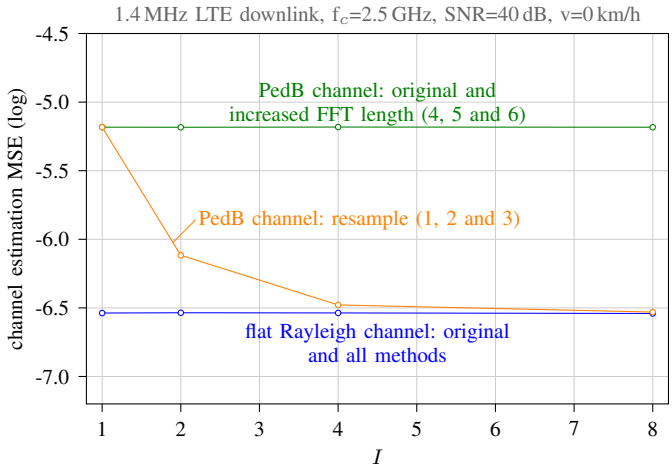

Fig. 3. The spectral channel estimation error decreases with decreasing pilot spacing in frequency selective channels. For a fixed pilot spacing the channel interpolation error is emulated correctly.

case where data symbols are repeated and are therefore not independent anymore.

B. Channel estimation error

All methods investigated here have in common that signals are stretched in time to emulate higher receiver velocities and therefore the spatial lengths of the resulting signals are exactly the same as for the original signal at the velocity to be emulated. This is also valid for the spatial pilot spacing and therefore for the resulting spatial channel interpolation errors. However, in the frequency domain differences arise. While the original pilot spacing is preserved for the methods that insert additional subcarriers, the pilot spacing decreases with I when resampling the original signal by the factor I. In order to focus on this spectral effect, we performed simulations at v=0 km/h and evaluated the mean squared channel estimation and interpolation error

$$MSE = \frac{1}{R}\frac{1}{N}\frac{1}{K}\sum_{r=1}^{R}\sum_{n=1}^{N}\sum_{k=1}^{K}\left|\widehat{H}_{n,k,r} - H_{n,k,r}\right|^2 . \quad (3)$$

$\widehat{H}_{n,k,r}$ denotes the estimated channel coefficient and $H_{n,k,r}$ is the actual channel coefficient at subcarrier k, time symbol n and channel realization r. Figure 3 shows the increased channel estimation error due to the frequency selectivity of the PedB channel compared to the frequency flat channel. As the absolute pilot spacing decreases with increasing I, for the methods based on resampling the channel estimation error decreases and converges to the error for the frequency flat channel.

C. Physical layer throughput

The physical layer throughput combines all the aforementioned effects. We use it as a metric for the applicability of the different methods to emulate higher velocities at lower velocities. In order to suppress the impact of feedback, usually necessary for link adaptation, we use a brute-force approach where all possible Modulation and Coding Schemes (MCSs) are transmitted over the same channel realization and the best performing MCS is chosen as the one an ideal feedback function would have chosen. The average physical layer throughput is then calculated as the average over all channel realizations r of the datarate of the respectively best performing MCS to

$$D(v, I) = \frac{I}{R}\sum_{r=1}^{R}\max_{\text{MCS}} D_r(v, I, \text{MCS}) . \quad (4)$$

In order to compare the emulated throughput rather than the actual throughput, the actual throughput is scaled with I as the symbol length increases with I and therefore the throughput decreases. Note that in order to focus on the impact of channel estimation and ICI, simulations were performed at SNR→ ∞. Figure 4 shows the results in terms of throughput as well as the relative error in relation to the results for the original signal. For the frequency flat channel (Figure 4a) the methods that repeat subcarriers have a lower throughput due to a lower SIR. All other methods emulate the higher velocities accurately in terms of throughput. That is different for the frequency selective PedB channel as shown in Figure 4b. Only the method that inserts random symbols emulates the higher velocities correctly. For the resample methods the throughput is higher than it should be as the pilot spacing decreases and therefore the channel estimation errors decrease with I.

IV. Practical Aspects

While simulations are a proper way to evaluate and compare the different methods proposed in this paper their intended use are in real world experiments where one has to cope with hardware limitations and impairments. In order to evaluate the impact of the effects of time varying mobile channels like channel interpolation errors and ICI the impact of other effects should be kept small compared to the effects under investigation. We were thereby interested in the effect of the different methods on the SNR and on the PAPR. For a

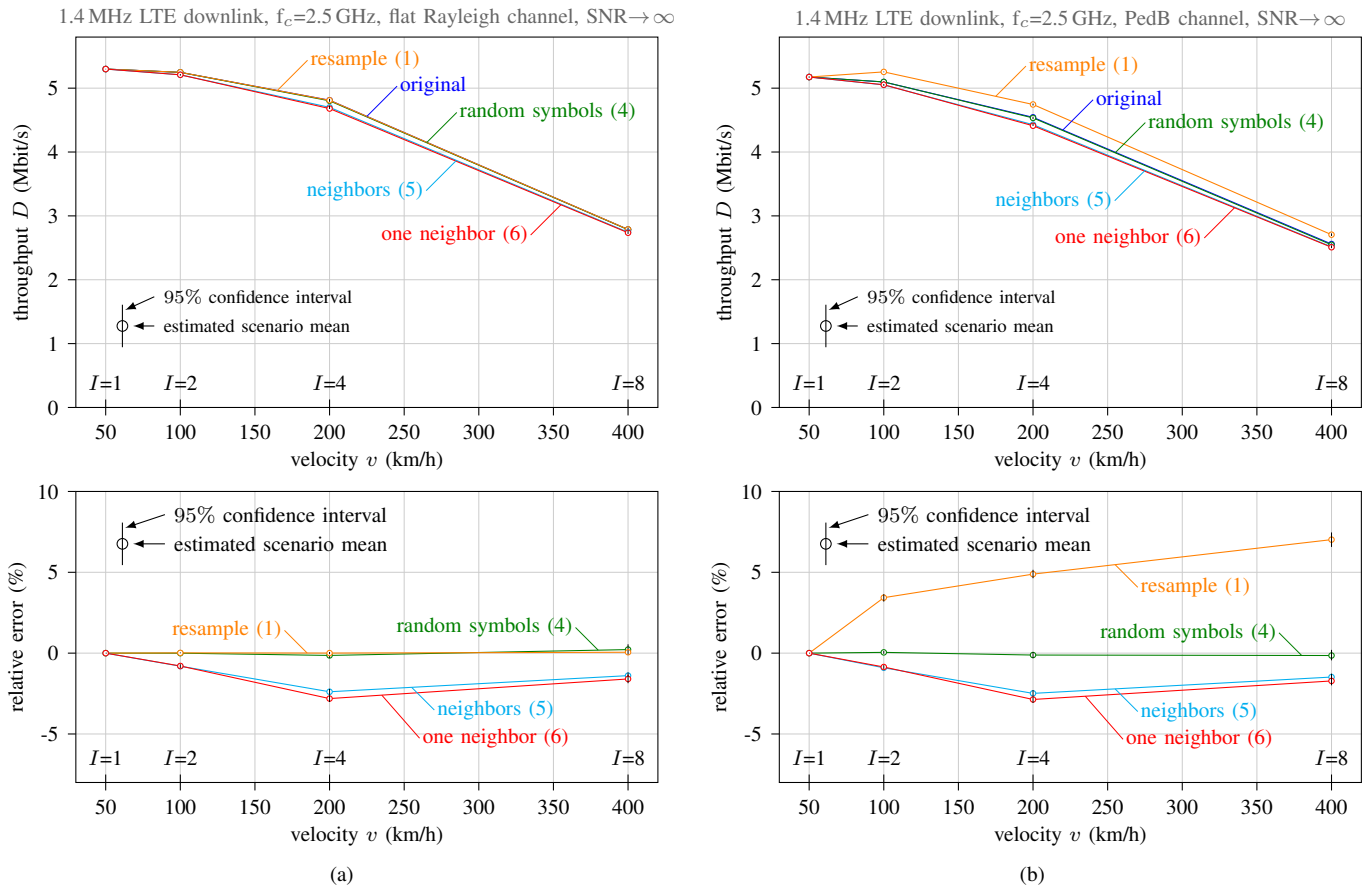

Fig. 4. (a) For a frequency flat channel the throughput for the methods that repeat data symbols is lower due to the lower SIR while all other methods perform well. (b) For the frequency selective PedB channel the throughput for the resample methods is too high due to the lower channel estimation errors.

given maximum transmit power the PAPR limits the maximum average transmit power and therefore also the SNR. On the other hand, for a given average transmit power, the ICI caused by nonlinearities in the transmission chain increases with increasing PAPR.

A. Signal to noise ratio

For the analysis of the SNR we evaluate the signal power and the noise power after the FFT in the OFDM demodulator since this definition of SNR is directly related to the effects of noise on data transmissions. Considering a transmission system with a fixed transmit power and zero-mean noise with fixed spectral density at the receiver, all methods have in common that the average per-subcarrier noise variance after the FFT[2] is independent of I and independent of the FFT length. That is different for the received signal power. For all methods except *method 1* the number of subcarriers increases with I and therefore the per-subcarrier transmit power decreases as the fixed total transmit power is equally allocated to all subcarriers. On the other hand, the symbol energy increases by I with increasing I for a fixed per-subcarrier transmit power as the symbol duration increases by I. Therefore a gain of SNR by a factor $g = \frac{I \cdot L}{L_t}$ is achieved whereas L denotes the initial number of subcarriers and L_t the number of subcarriers transmitted. For the methods that insert additional subcarriers we achieve a very small[3] gain of $g = \frac{I \cdot L}{I \cdot (L-1)+1} > 1$. The methods that resample and repeat, where $L_t = I \cdot L$, g=1, while the resample method achieves a gain of I as the number of subcarriers is not increased.

B. Peak to average power ratio

For the evaluation of the PAPR a per-symbol search for the peak power with oversampling factor J=4 [12] is performed. Different signals can then be compared by plotting the statistics of the peak powers in terms of an Complementary Cumulative Distribution Function (CCDF) as illustrated for three different signals in the embedded subplot of Figure 5. In order to compare all different methods for different values of I, we determine the value of PAPR that is exceeded by 1% of the OFDM symbols. Figure 5 shows the thereby obtained results. While resampling does not change the PAPR, repeating the same resampled signal results in a strong increase of the PAPR as data symbols are repeated. This effect vanishes

[2]When using a $\frac{1}{\sqrt{N}}$ scaling: $X[k] = \frac{1}{\sqrt{N}} \sum_{n=0}^{N-1} e^{-j2\pi \frac{kn}{N}} \cdot x[n]$

[3]For L=72 subcarriers and I=8, g=0.0531 dB .

TABLE I
CONCLUSION

	method	$I \in$	bandwidth	SNR	SIR	pilot spacing	neighboring subcarriers	PAPR	scenarios	ICI cancellation
1	resample	$\mathbb{R}_{>0}$	-	$\propto I$	+	-	+	+	low delay spread	+
2	resample & repeat same	$\mathbb{N}_{>1}$	(+)	$=$ const.	+	-	+	-	low delay spread	+
3	resample & repeat	$\mathbb{N}_{>1}$	(+)	$=$ const.	+	-	+	+	low delay spread	+
4	insert random symbols	$\mathbb{N}_{>1}$	+	$\approx$ const.	+	+	-	+	all	-
5	repeat neighbors	$\mathbb{N}_{>1}$	+	$\approx$ const.	-	+	(+)	-	all	(+)
6	repeat one neighbor	$\mathbb{N}_{>1}$	+	$\approx$ const.	-	+	(+)	(+)	all	(+)

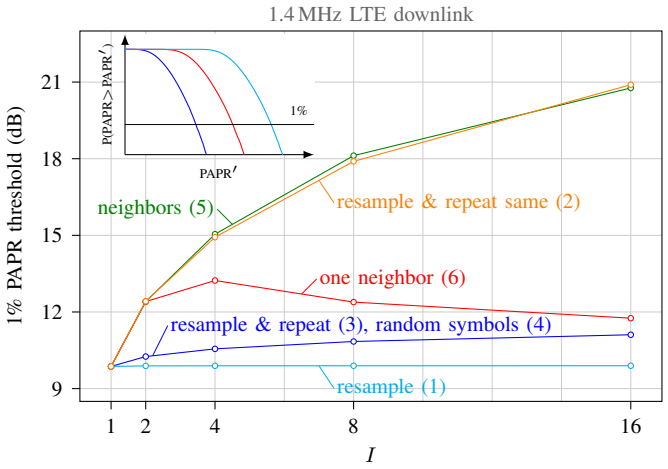

Fig. 5. Repeating subcarriers causes a strong increase of PAPR while when increasing the number of subcarriers and keeping the symbols random only a slight increase of PAPR is observed.

when different signal realizations[4] are used for the copies. The effect that the PAPR increases with increasing number of subcarriers remains as for the method where random symbols are inserted. Copying neighboring subcarriers yields similar results as copying the same signal. The PAPR is reduced by copying just the next neighbor and filling the remaining subcarriers with random symbols.

V. CONCLUSION

In Table I we see, that among the methods considered, there is no perfect technique to emulate high velocity LTE downlink transmissions at lower velocities. It depends on the scenario, the application and the intended implementation effort which method to use. Simply resampling the transmit signal is very easy to implement and allows for measurements at higher effective SNRs. In order to transmit with the correct bandwidth, the resampled signal can be repeated over frequency. The pilot spacing is still smaller than for the original signal. Transmissions with correct spectral properties are achieved by inserting random subcarriers. With this method, the average ICI is emulated correctly but not the actual ICI. The methods that try to emulate the correct ICI by inserting the correct subcarriers generate ICI that is higher than the intended ICI.

[4]If we consider different data symbols and different values for the pilots by using different LTE Cell IDs the subcarriers are completely independent.

Note that our considerations and findings are not limited to the LTE downlink. They can be applied to any multicarrier technique.

ACKNOWLEDGMENTS

This work has been funded by the Christian Doppler Laboratory for Wireless Technologies for Sustainable Mobility, KATHREIN Werke KG and A1 Telekom Austria AG, as well as Xunta de Galicia, MINECO of Spain, and FEDER funds of the EU under grants 2012/287, IPT-2011-1034-370000, TEC2013-47141-C4-1-R, CSD2008-00010, FPU12/04139, EST13/00272, and EST14/00355. The financial support by the Austrian Federal Ministry of Economy, Family and Youth and the National Foundation for Research, Technology and Development is gratefully acknowledged.

REFERENCES

[1] P. Robertson and S. Kaiser, "The effects of Doppler spreads in OFDM (A) mobile radio systems," in *IEEE Vehicular Technology Conference, Fall*, vol. 1. IEEE, 1999, pp. 329–333.

[2] 3rd Generation Partnership Project (3GPP), "Evolved Universal Terrestrial Radio Access (E-UTRA) physical channels and modulation," TS 36.211, 2015.

[3] J. Rodríguez-Piñeiro, P. Suárez-Casal, J. A. García-Naya, L. Castedo, C. Briso-Rodríguez, and J. I. Alonso-Montes, "Experimental Validation of ICI-Aware OFDM Receivers under Time-Varying Conditions," in *IEEE 8th Sensor Array and Multichannel Signal Processing Workshop (SAM'2014)*, A Coruña, Spain, Jun. 2014.

[4] P. Suárez-Casal, J. Rodríguez-Piñeiro, J. A. García-Naya, and L. Castedo, "Experimental Evaluation of the WiMAX Downlink Physical Layer in High-Mobility Scenarios," *EURASIP Journal on Wireless Communications and Networking*, no. 109, Dec. 2015.

[5] J. Rodríguez-Piñeiro, M. Lerch, J. A. García-Naya, S. Caban, M. Rupp, and L. Castedo, "Emulating Extreme Velocities of Mobile LTE Receivers in the Downlink," *EURASIP Journal on Wireless Communications and Networking*, no. 106, 2015.

[6] J. Rodríguez-Piñeiro, M. Lerch, P. Suárez-Casal, J. A. García-Naya, S. Caban, M. Rupp, and L. Castedo, "LTE Downlink Performance in High Speed Trains," in *Proceedings of the 81st Vehicular Technology Conference (VTC2015-Spring)*, Glasgow, Scotland, May 2015.

[7] C. Mehlführer, J. C. Ikuno, M. Šimko, S. Schwarz, M. Wrulich, and M. Rupp, "The Vienna LTE Simulators - Enabling Reproducibility in Wireless Communications Research," *EURASIP Journal on Advances in Signal Processing*, vol. 2011, pp. 1–13, 2011.

[8] [Online]. Available: http://www.nt.tuwien.ac.at/ltesimulator/

[9] T. Zemen and C. Mecklenbräuker, "Time-Variant Channel Estimation Using Discrete Prolate Spheroidal Sequences," *Signal Processing, IEEE Transactions on*, vol. 53, no. 9, pp. 3597–3607, Sept 2005.

[10] Y. Zheng and C. Xiao, "Simulation models with correct statistical properties for Rayleigh fading channels," *Communications, IEEE Transactions on*, vol. 51, no. 6, pp. 920–928, June 2003.

[11] 3rd Generation Partnership Project (3GPP), "High speed downlink packet access: UE radio transmission and reception," TR 25.890, 2002.

[12] T. Jiang and Y. Wu, "An Overview: Peak-to-Average Power Ratio Reduction Techniques for OFDM signals," *Broadcasting, IEEE Transactions on*, vol. 54, no. 2, pp. 257–268, June 2008.